5-2024

Redesign of X-Ray Irradiator to Expand Research of Low-Dose X-Ray Radiation

Lauren Ulbrich
lulbric@clemson.edu

Redesign of X-Ray Irradiator to Expand Research of Low-Dose X-Ray Radiation

---

A Thesis
Presented to
the Graduate School of
Clemson University

In Partial Fulfillment
of the Requirements for the Degree
Master of Philosophy
Physics

---

by
Lauren Ulbrich
May 2024

Accepted by:
Dr. Endre Takacs, Committee Chair
Dr. Delphine Dean
Dr. Joan Marler

Abstract

The effects of high-dose radiation are well-documented, and are understood to be harmful to the human body. On the other hand, the effects of low-dose radiation are much less understood. There is debate over whether or not there are negative, positive, or no effects at all from low-dose radiation. One of the reasons why these effects are not well known is because there aren't as many studies done on this type of radiation. It is a lot harder to classify the effects of radiation at low doses due to many external factors. However, the Clemson Medical Physics lab has been at the forefront of low-dose x-ray radiation research.

The lab has designed a device that reduces the effects of outside influence, and is able to irradiate cells with highly characterized x-rays to deliver low-dose radiation with great accuracy. One downside to the device, however, was that it was limited in the dose that it can impart, only being able to deliver a few mGy before overheating.

A new set-up was developed in order to expand the range of doses that it can impart on cells. These changes involved moving the x-ray source so it directly hits the target with bremsstrahlung x-rays, and adding in a filter feature to allow for extra control of the x-rays delivered. Preliminary results show that the system is in working order, although users need to be careful to avoid over-saturating the detector to prevent double and triple counting of photons.

Dedication

To my parents, Chris and Lynn, thank you for your continuous support through my academic journey. Whether I'm working at my desk at home or 12 hours away, I know you'll always be there.

To Jacob and Brianna, thanks for the countless phone calls, messages of encouragement, and pictures of Barry and Louie!

To all my friends, thanks for all the game nights, book clubs, and hangouts throughout the years keeping me sane while I worked.

To all my D&D party members, thanks for your support. I rolled a nat 20 on my intelligence check!

Acknowledgments

I would first like to thank my advisor, Dr. Endre Takacs. I still remember the day that you first presented in my physics seminar course and reached out to me afterwards to gauge my interest in your research. If you had told me back then how far I would have gotten, I don't know if I would have believed you, but with your encouragement and support I was able to go above and beyond. You have also been so supportive in helping me find the path that I want to take in my career, and for that I am truly grateful.

I would also like to thank my committee members, Dr. Delphine Dean and Dr. Joan Marler. You were both there to step up and support me when I needed you the most, and for that I thank you so much. I appreciate you being there for me as I went through my academic journey.

I would like to extend my thanks to the Radiation Creative Inquiry group. This group consistently inspired my research and supported me throughout all of my plans. It is because of you that I even wanted to redesign our irradiator in the first place, so thank you for being that point of inspiration! I would like to give a special shout out to Arianna Csiszer and Calvin Paulsen, who have been an incredible help throughout my time in the group!

A HUGE thank you to Barrett Barker of the Clemson Physics and Astronomy machine shop. It was because of you that any of my research was even possible. You helped me through countless upgrades and redesigns; without your expertise, the irradiator would not be where it is today.

Finally, many thanks to the Clemson Physics and Astronomy Department. I have learned so much during my time here, and have gotten so much help from both my peers and the faculty and staff. Thank you for your consistent support as I grew as a scholar and a physicist.

Table of Contents

List of Tables

List of Figures

Chapter 1

Introduction

When looking at the effects of radiation on the human body, it is well accepted that high doses of radiation (>1 Gy) have negative effects. Between acute radiation poisoning, severe burns on the skin, and an increased risk of cancer, there are a multitude of ways that high dose radiation can induce harm in the body [1][2][3][4]. However, it is currently unclear what the effects of radiation may be in low doses. In fact, for low-doses (<100 mGy) or even some mid-range doses (100 mGy - 200 mGy), there are results indicating negative responses in some cases, and others positive [5][6]. There are multiple models that have been created to try and describe the effects of low-dose radiation on cells. These predictions can be shown using a dose-response curve, as shown in Figure 1.1. In each model, the thin, flat line represents no response from cells, with curves falling below the line indicating a positive response and curves above the line indicating a negative response.

The first model presented is known as the threshold model. According to this curve, there is no effect on cell response before a certain radiation dose. Then, once the radiation threshold is reached, harmful responses are found to increase as the dose increases. There is also a subset of threshold curves not shown in the figure, known as sigmoid, or S-shaped, curves. They start off the same, showing no radiation effects below the threshold dose, and once the threshold is reached the response starts to grow along with the dose. However eventually a maximum response is obtained and afterwards the curve will flatten. It is predicted that the maximum response is a result of the irradiated cells dying after reaching a certain dose. The second model shown is the linear model. This curve indicates that there is always a negative effect due to radiation exposure no matter how little dose is received, and that the response is directly proportional to the total dose. The third

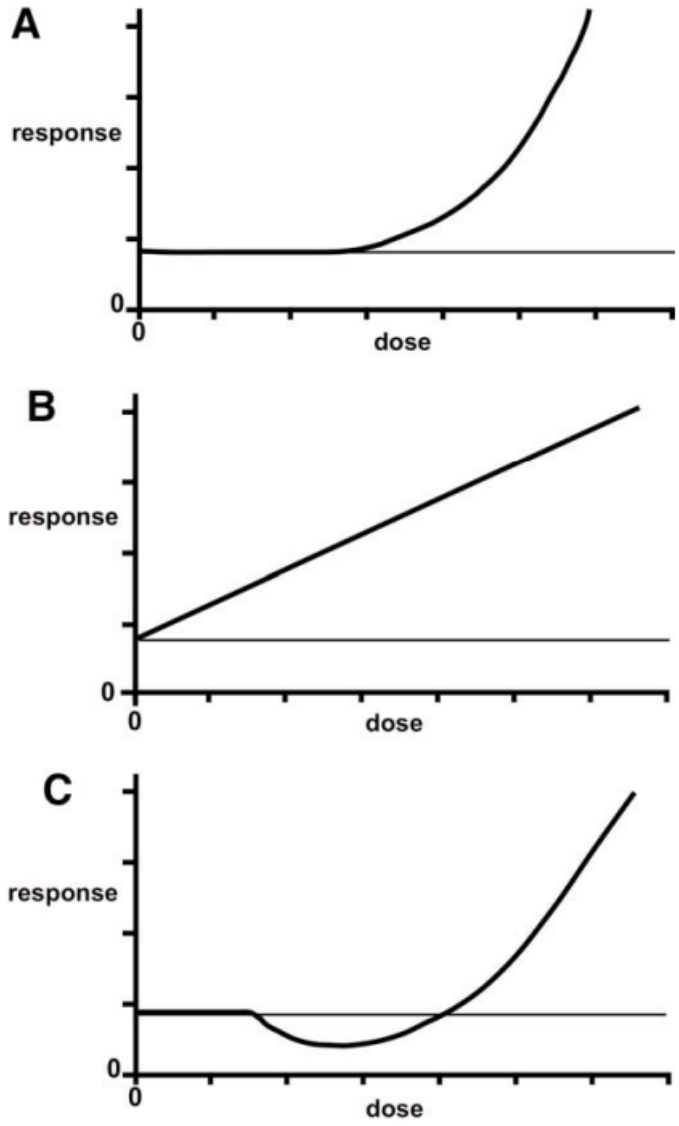

Figure 1.1: Three potential dose-response models. (A) represents a Threshold curve (B) represents a Linear curve, and (C) represents the Hormesis model [7].

model shown is the hormesis model. This model starts off with little to no effect, then for certain lower doses it shows radiation having a beneficial effect before moving back to harmful effects after a certain dose is reached. These beneficial effects may include responses like helping with cell repair, or preventing certain DNA damage [8]. All these models agree with the behavior of cells at high doses, the differences are in the uncertainty of behaviors at low doses.

The reason it is so hard to predict the response of cells at low doses is because it is a lot harder to quantify the effects of radiation. At low doses it can be hard to tell whether or not an effect is due to environment, set up, cell type, etc., or if it is actually an effect from the radiation, so many researchers tend to focus on more deterministic results at higher doses, and write off low-dose effects as stochastic, or random [4]. However, experiments performed at the Clemson University Medical Physics Lab have previously been able to narrow down some of these extraneous variables to study cell response at low doses.

1.1 Previous Experiment Done At The Clemson University Medical Physics Lab

In the Clemson Medical Physics Lab, an x-ray irradiator was developed to study the effects of low-dose x-rays on cells, with great success. The original purpose of the irradiator was to push the boundaries of the field by using highly characterized, quasi-monochromatic fluorescent x-rays to irradiate targets with low-dose radiation.

In one study done in the lab, the effects of low-dose radiation on 3T3 fibroblast cells were determined by irradiating the cells at a dose rate of 550 μGy/hr for a total of 550 μGy. It was found that after the irradiation there was an initial pause in cell production, followed by a sharp increase in cell proliferation, as shown in Figure 1.2. It was also indicated through cell staining that irradiated cells maintained normal cell functions after radiation exposure. The results of this study suggest that the pause in the cell proliferation could be a protective mechanism of the cells to minimize DNA damage caused by radiation exposure [9].

These highly characterized x-rays make it easy to calculate an accurate dose rate, however the device was limited in the doses that it could impart onto cells. In that set-up, it could only produce dose rates of less than 1 mGy/min, and this could only be sustained for very short periods of time before the device starts to overheat and potentially damage both the electronics in the x-ray

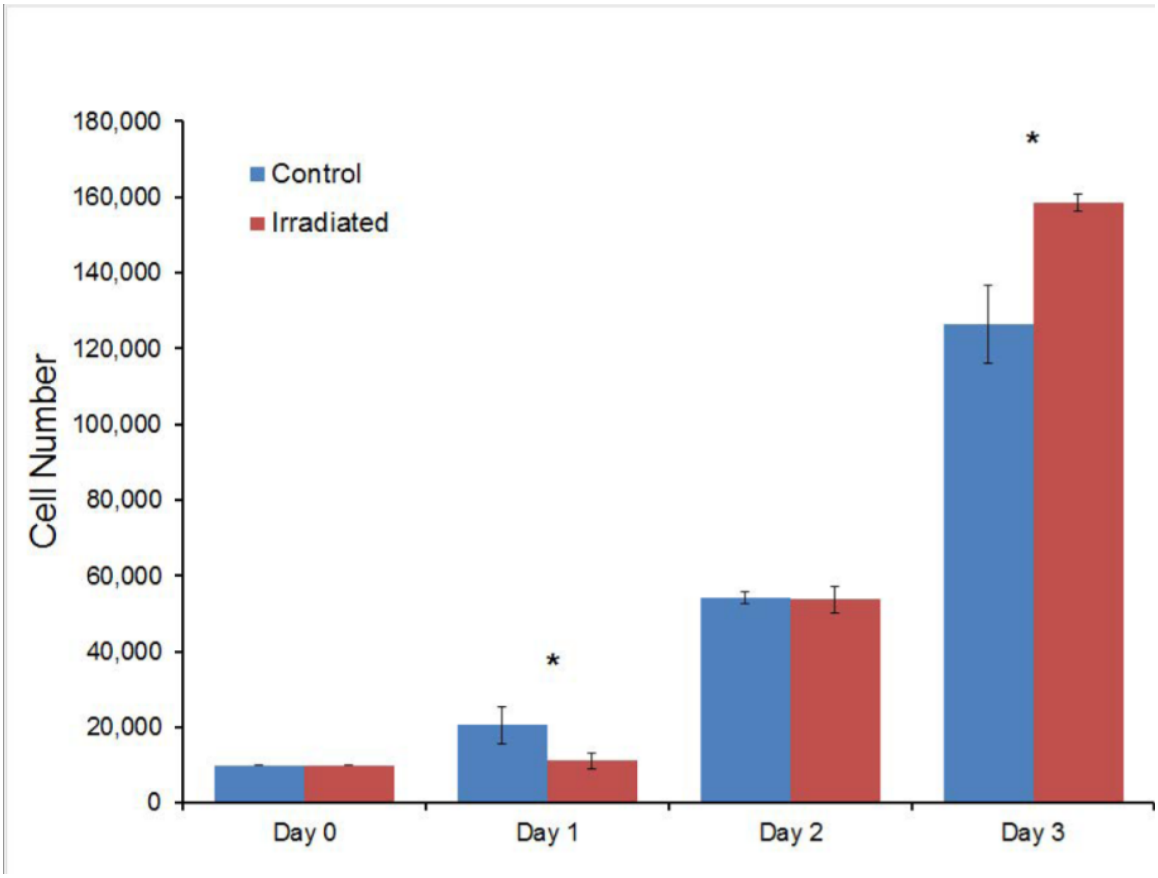

Figure 1.2: Cell proliferation for control group and cells irradiated for 550 μGy [9].

source and the cells inside. At this maximum state the irradiator can only deliver a total dose of only a few mGy (<10 mGy) before reaching this critical temperature.

1.2 Research Objectives

The purpose of my research is to increase the amount of energy that can be imparted on the cells, so that research can be done on a wider range of dose rates and total doses. This was done by redesigning the low-dose x-ray cabinet, as well as developing a way to analyze the spectra produced in this new set-up. I also wanted the design to be reversible, so it could switch between the original set-up and new set-up with ease. In doing so, this allows the irradiator to deliver higher dose rates and total doses, while still being able to switch back and deliver characteristic x-rays to cells if desired.

Chapter 2

Physics of Radiation

The science of radiation touches on many different aspects of physics. It is important to understand the basics of radiation before performing any irraditaion experiment, especially one that may have an impact on the human body. Through a thorough understanding of the physics of radiation, experiments can be performed in a safe manner on humans, which can protect both the experimenter and any patient from unnecessary harm.

2.1 Ionizing vs Non-Ionizing Radiation

Radiation is classified into two categories, depending on the amount of energy that it has: ionizing radiation and non-ionizing radiation.

Ionizing radiation has the ability to knock electrons out of an atom's orbit, giving the atom a positive charge and making it an ion. In order to do this, the radiation must have a higher energy than the minimum ionization energy of the atom. This type of radiation can be further split into two categories, directly ionizing radiation and indirectly ionizing radiation [10]. Directly ionizing radiation deposits energy through Coulomb interactions between the atom and the radiation particle. This can include radiation from any charged particle, such as electrons, protons, α particles, and other heavy ions. Indirectly ionizing radiation occurs in two steps: first, a neutral particle will impart energy through the production of a charged particle by collision. This newly produced charged particle then has a Coulomb interaction with the atom. Indirectly ionizing radiation is generally produced through photons, and occurs only with photons which have a high enough energy: some

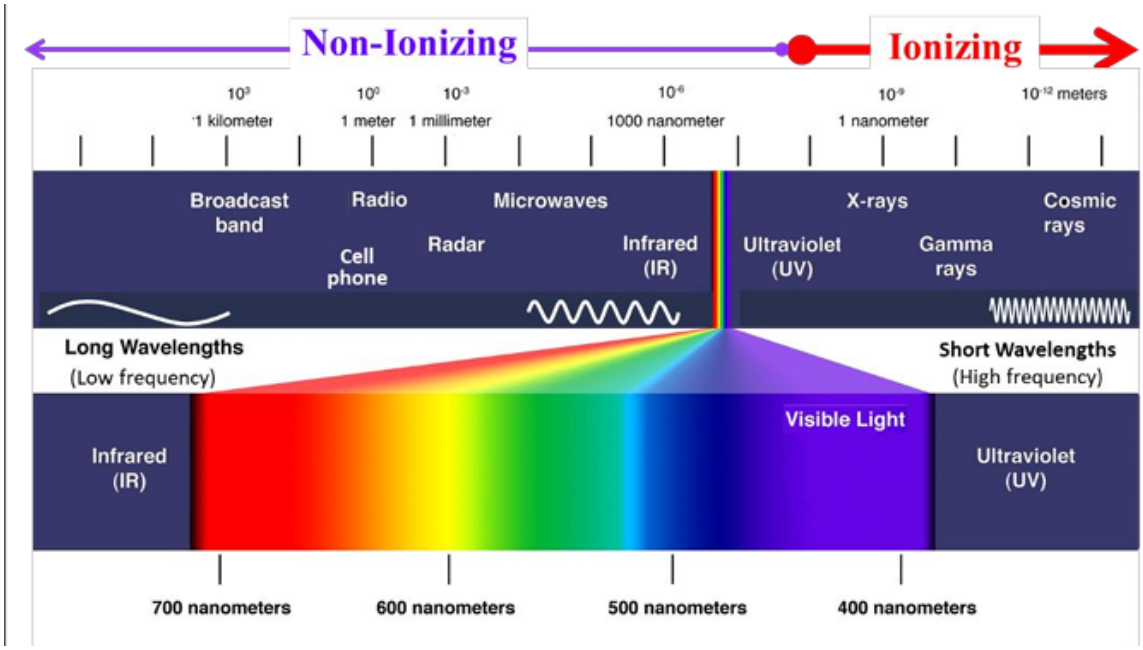

Figure 2.1: A chart of the electromagnetic spectrum, which indicates ionizing versus non-ionizing radiation [12].

ultraviolet, x-rays, and gamma rays [11].

Non-ionizing radiation is any radiation that does not have enough energy to reach above the minimum ionization energy of the atom. Because of this, it does not have enough energy to damage DNA or break cells. Examples of non-ionizing radiation include radio waves, microwaves, infrared, and visible light [10]. Figure 2.1 shows a chart of the electromagnetic spectrum, indicating which type of radiation is ionizing and non-ionizing.

For the purposes of this research, I mainly focus on indirectly ionizing radiation, as my work delivers energy to cells through x-rays. Now that it is understood what type of radiation is being used, it is important to understand what x-rays are and what properties they have.

2.2 Understanding X-rays

X-rays are a small fraction of what is known as the electromagnetic spectrum, as seen in figure 2.1. Light can be described as wave-like, yet it also comes in discrete packages called photons in a phenomenon known as the wave-particle duality [13]. Certain phenomena are best understood considering a wave-like picture, where the light travels in the direction of the propagation vector

that is orthogonal to the oscillations of the electric and magnetic fields [14]. This behavior is seen at a more macroscopic scale, and is not the focus of this research. On a more atomic scale, light is seen as photons, and acts particle-like. Photons have an energy that is proportional to their frequency. This relationship is described by the Planck-Einstein equation:

$$E = h\nu = \frac{hc}{\lambda} \tag{2.1}$$

where E is the energy, ν is the frequency, h is Planck's constant, c is the speed of light, and λ is the wavelength [13]. X-rays are found to be in an energy range of 10 eV to 100 keV [15].

X-rays are generally produced two different ways, as characteristic x-rays and bremsstrahlung x-rays. Each type is produced in a very different way, and produces very different results, so it is important to understand the distinctions between the two.

2.2.1 Characteristic X-rays

Characteristic x-rays are produced as a result of transitions between electrons in orbit around a nucleus. As seen in Figure 2.2, orbital electrons around an atom generally tend to inhabit the shell that results in the minimum energy state for the atom. However, if one of these electrons becomes excited or ionized, it leaves a vacancy in its place within the shell. In this case, an electron in an outer shell will transition to fill that spot. When this transition happens, there is energy that is released in the form of a characteristic, or fluorescent, photon with energy equal to the difference between the binding energies of the initial and final position. The reason these x-rays are called characteristic x-rays is because they are unique to each atom: each element has different binding energies for each of their shells. So, if we know the element that is releasing these x-rays, it is very easy to determine what energies the fluorescent photons will have. It is also important to note that because the photons can only come from these specific shell transitions, the energies of the x-rays produced will be discrete [11]. An example of the discrete energy spectra produced is seen in Figure 2.2.

2.2.2 Bremsstrahlung X-rays

The phrase bremsstrahlung comes from the German words "bremsen" meaning "to brake" and "strahlung" meaning "radiation", combining to mean "braking radiation" [17]. This is very

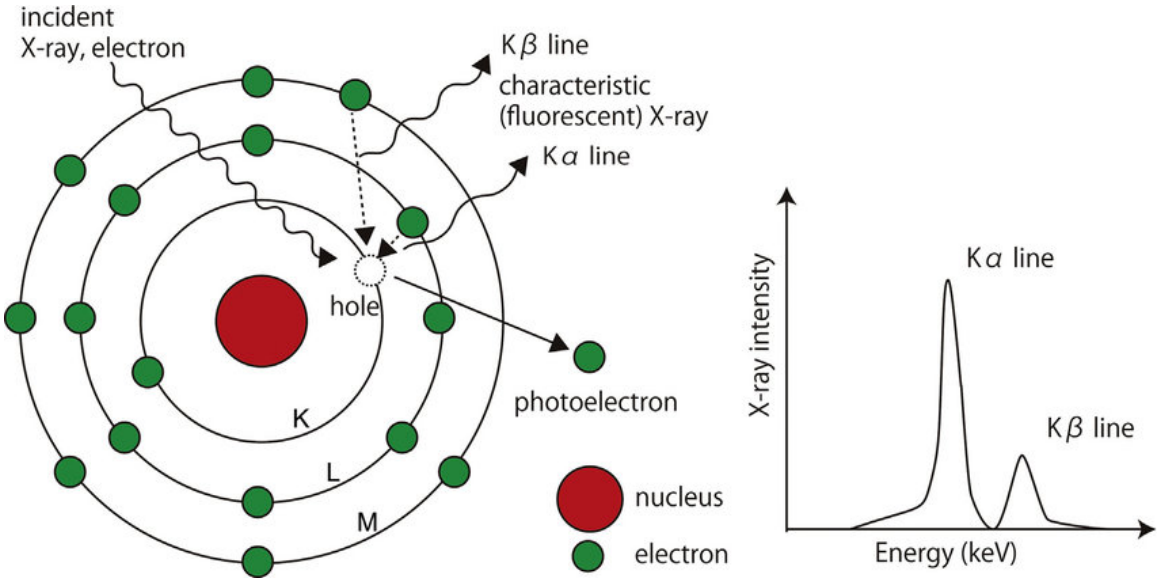

Figure 2.2: Demonstration of characteristic x-ray production, and the resulting discrete energy spectra [16].

fitting, as the radiation is created through the slowing down of fast-moving electrons. As seen in Figure 2.3, when negatively-charged electrons pass by positively charged nuclei, they are decelerated through the interaction, and the lost kinetic energy is released as a photon. The resulting energy of that photon can range from zero to the original kinetic energy of the electron, meaning that the energy spectrum produced by bremsstrahlung radiation is continuous. Bremsstrahlung is very important in modern medical physics equipment, as it is very easy to produce these x-rays from an electrical energy source [11]. Now that the basics of x-rays has been covered, its is important to study how to measure the energy that gets imparted by this radiation

2.3 Radiation Dosimetry

Radiation dosimetry is a procedure that deals with the quantitative determination of energy deposition in a medium [18]. Accurate measurement of the radiation is of utmost importance in medical physics to both ensure the optimization of procedures and to prevent any unnecessary harm from occurring. To aid in this measurement, several quantities are needed to help understand the effects of radiation on the body.

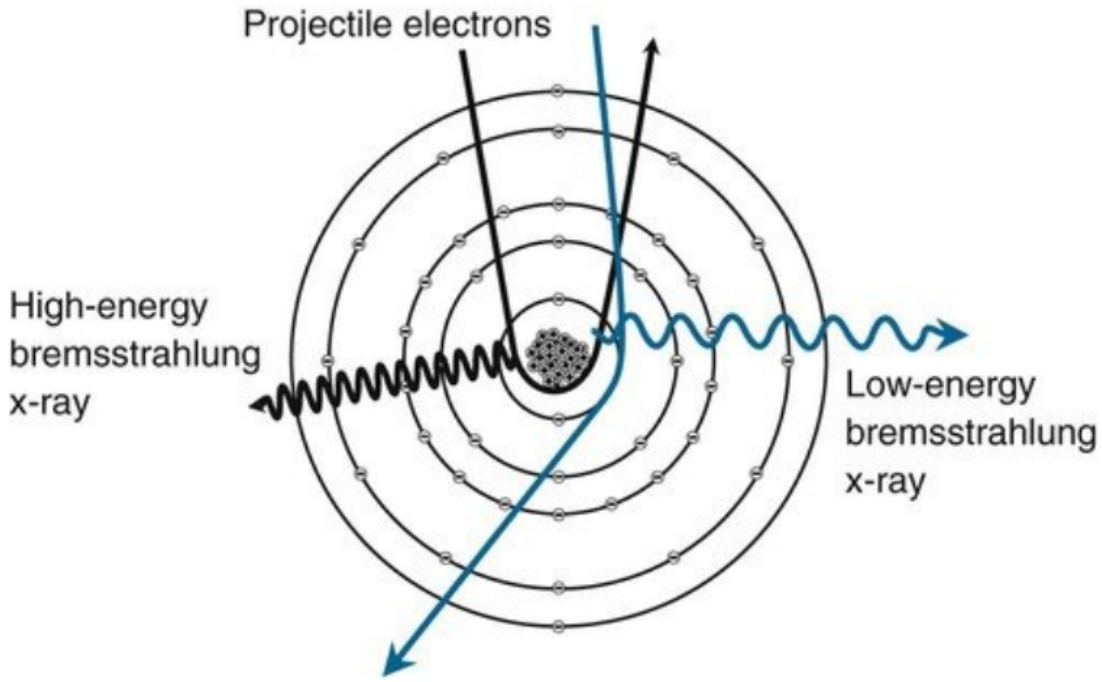

Figure 2.3: Demonstration of both high-energy and low-energy bremsstrahlung x-ray production [17].

2.3.1 Fluence

Fluence is defined as the flux of radiation particles or energy intersecting a unit area over a period of time. For a mono-energetic radiation beam, the particle fluence, Φ, can be written as

$$\Phi = \frac{dN}{dA} \tag{2.2}$$

where dN is the number of incident particles, and dA is the cross-sectional area. The energy fluence, Ψ, can be written as

$$\Psi = \frac{dR}{dA} \tag{2.3}$$

where dR is the radiant energy incident on the cross-sectional area dA. For the mono-energetic radiation beam, R is the product of the number of particles, N, and their energy, E, leading to the following relation:

$$dR = dNE \tag{2.4}$$

This allows for the particle fluence and energy fluence to be related in the following way:

$$\Psi = \frac{d(NE)}{dA} = (\frac{dN}{dA})E = \Phi E \tag{2.5}$$

The units of particle fluence are number of particles per m^2 ($\#/m^2$), and the units for energy fluence are Joules per m^2 (J/m^2) [18].

2.3.2 KERMA

Kerma is an acronym standing for "kinetic energy released in matter". For indirectly ionizing radiation like x-rays, kerma is defined as the energy transferred to charged particles per the unit mass of the absorber [11]. The energy transferred by the radiation can be used in two ways, known as collisional kerma and radiative kerma. The relationship between the two types is as follows:

$$K = K_{col} + K_{rad} \tag{2.6}$$

where K is the total kerma, K_{col} is the collisional kerma, and K_{rad} is the radiative kerma. Collisional kerma is the portion of energy that is spent in collisions resulting in the ionization and excitation of the target atom. Radiative kerma is the portion of energy that is converted into photon energy. For a photon with an energy E, the following equation can be used to relate the kerma and the fluence:

$$K = \Phi E(\frac{\mu_{tr}}{\rho}) = \Psi(\frac{\mu_{tr}}{\rho}) \tag{2.7}$$

where $\frac{\mu_{tr}}{\rho}$ is the mass energy transfer coefficient. Kerma is material-dependent, so it is important to state the target material when measuring kerma. Kerma is measured in units of Gray (Gy), which in SI units 1 Gy is defined as 1 Joule per kilogram (J/kg) [19].

2.3.3 Exposure

When high energy photons, like x-rays, interact with matter, it can produce ion pairs in the air. The amount of ion pairs can be measured in a quantity called exposure. The exposure is defined

as the total charge produced by ionizing radiation in air of a certain mass, and is represented with the following relation:

$$X = \frac{dQ}{dm} \tag{2.8}$$

where X is the exposure, dQ is the total charge, and dm is the mass [18]. Exposure has SI units of Coulomb per kilogram (C/kg) in air, however it cab also be measured in Roentgens (R), which is defined as 2.58×10^{-4} coulombs produced per kilogram of air [11]. Exposure is important as it is proportional to the energy fluence, and can be used to help determine absorbed dose in other medium [18]. It can also be related to collisional kerma through the following relation:

$$(K_{col})_{air} = \overline{W}_{air} X \tag{2.9}$$

where $(K_{col})_{air}$ is the collisional kerma of air, $\overline{W}_{air}$ is the mean energy spent in air to form an ion pair, and X is the exposure. The value for $\overline{W}_{air}$ is equal to 33.97 J/C [19].

2.3.4 Dose

The dose, also known as the absorbed dose, is the average energy that is absorbed per unit mass of medium. As a general equation, it can be written as

$$D = \frac{\Delta E}{\Delta m} \tag{2.10}$$

where D is the dose, ΔE is the energy, and Δm is the mass of the target [11]. For a number of photons N of energy E hitting a target of total mass M, the average energy will be equal to the number of particles times the energy of the photon, or $\Delta E = NE$. From this, the absorbed dose equation can be rewritten as the following.

$$D = \frac{NE}{M} \tag{2.11}$$

The previous equation is for a mono-energetic x-ray. If there is a range of particle energies, the dose ends up being the sum of each individual photon energy multiplied by the number of incident photons with that energy.

$$D = \sum_i \frac{N_i E_i}{M} \tag{2.12}$$

The units of the absorbed dose are Gy, similar to kerma.

2.3.5 Equivalent Dose

The equivalent dose is based on the absorbed dose. The equivalent dose takes into account both the dose absorbed by the target, and a radiation weighting factor that is a unitless quantity dependent on the type and energy of the radiation. It is described by the following equation:

$$H_T = Dw_r \tag{2.13}$$

where H_T is the equivalent dose, D is the absorbed dose, and w_r is the radiation weighting factor [11]. The equivalent dose has units of sieverts (Sv), and is generally used in biological settings [8].

2.3.6 Effective Dose

The effective dose is also used in biological settings, it is generally used to describe the more long-term effects a particular type of radiation has on the body. It expands upon the equivalent dose, multiplying it with a tissue weighting factor. The tissue weighting factor is material-dependent; each tissue reacts in a unique way to different radiation. It can be described with the following equation:

$$E = H_t w_t \tag{2.14}$$

where E is the effective dose, H_t is the equivalent dose, and w_t is the tissue weighting factor [11]. The effective dose is also measured in Sv, similar to the equivalent dose. Radiation doses are generally measured in mSv; an effective dose of one Sv or higher can lead to severe health effects [8].

2.3.7 X-ray Attenuation

Another important quantity to consider when studying how x-rays interact with material is attenuation. Attenuation determines how the photon beam energy decreases, or eventually gets totally dissipated, over time as it passes through and exits a medium. The intensity of an x-ray beam that passes through a medium can be described by the following equation:

$$I(x) = I(0)e^{-\mu x} \tag{2.15}$$

where I(x) is the intensity at the absorber thickness x, I(0) is the initial intensity before the absorber, and μ is the attenuation coefficient.

The attenuation length, $\bar{x}$, is defined as the thickness of the absorber that attenuates the initial beam intensity by 1/e. This length is related to the attenuation coefficient, and can be derived like so [11]:

$$I(x) = \frac{1}{e}I(0) = I(0)e^{-\mu\bar{x}} \tag{2.16}$$

$$\frac{1}{e} = e^{-\mu\bar{x}} \tag{2.17}$$

$$\mu\bar{x} = 1 \tag{2.18}$$

Chapter 3

Redesign of Irradiator

The original purpose of the irradiator was to design a standardized, low-dose x-ray device that could be replicated by any research facility to perform research on the biological effects of low-dose radiation. Therefore, it was built in a way that any lab could easily purchase or make modifications to the machine to adapt to their research goals. In my current research, I endeavored to continue that standard, so any modifications made could be easily replicated in any lab.

3.1 X-ray Irradator Box

The x-ray irradiator was designed to be small enough to sit inside of a standard commercial incubator. The incubator used in the Clemson Medical Physics lab is the Fisherbrand^{TM} Isotemp^{TM} Direct Heat CO2 Incubator [20], as seen in Figure 3.1. This incubator was chosen, as it allows for regulation of temperature, humidity, and CO_2 concentration to help keep cells viable for up to 72 hours. Its interior chamber is 54.1 cm $\times$ 68.1 cm $\times$ 50.8 cm, or 184 L, and it is composed of stainless steel. It also includes a HEPA filtration system, allowing for easy sterilization of the environment to prevent any cross-contamination of cells. Any person that works inside of the incubator must wear gloves, and anything that goes into the incubator (besides the cell targets) must be sterilized with 70% ethanol, as seen in the warning placard in Figure 3.1. Also, for the safety of the operator, a magnetic interlock was attached to the outer incubator door. The interlock must be locked to start the irradiator, otherwise the x-ray tube will not turn on. This enforces extra shielding between the operator and radiation produced when the irradiator is on.

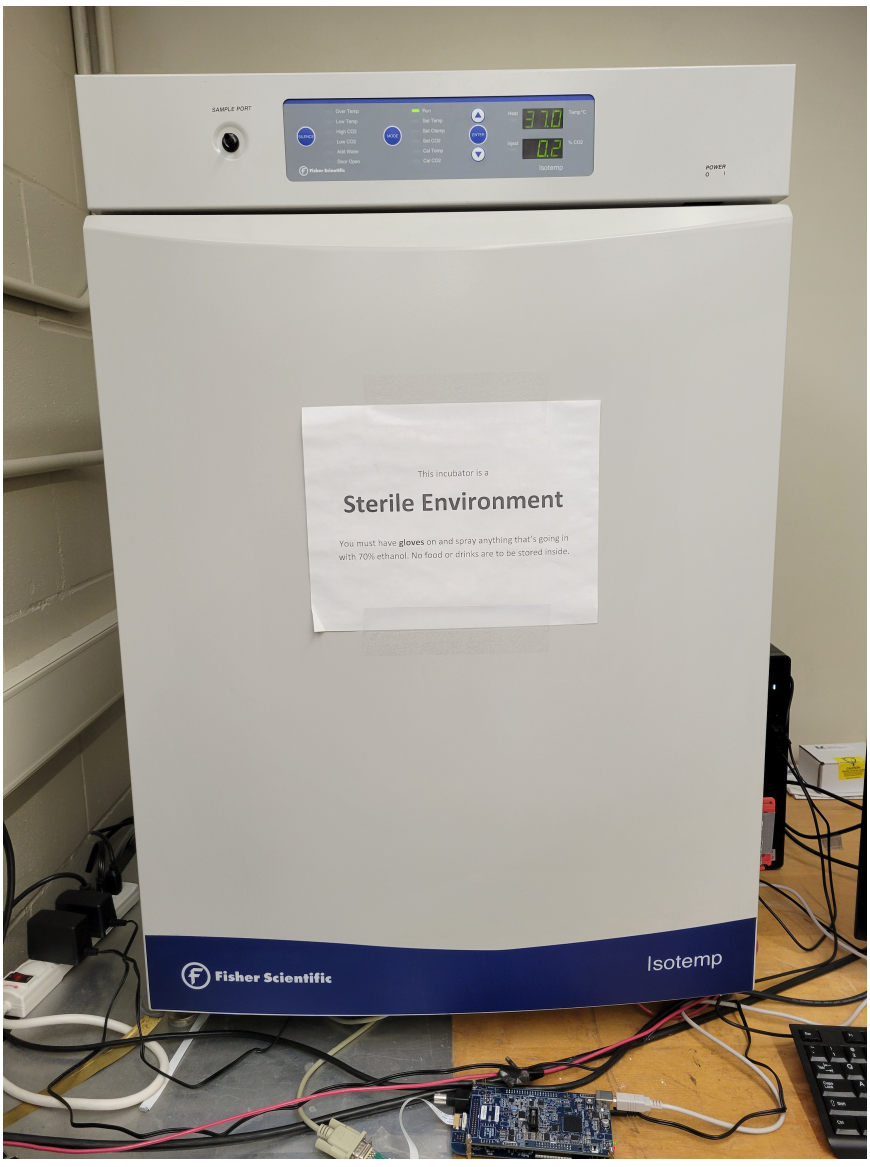

Figure 3.1: The Fisherbrand^{TM} Isotemp^{TM} Direct Heat CO2 Incubator inside of the Clemson Medical Physics lab [20]. On the door there is a warning placard reminding users to wear gloves and sterilize, and in the bottom right corner there is an orange magnetic interlock.

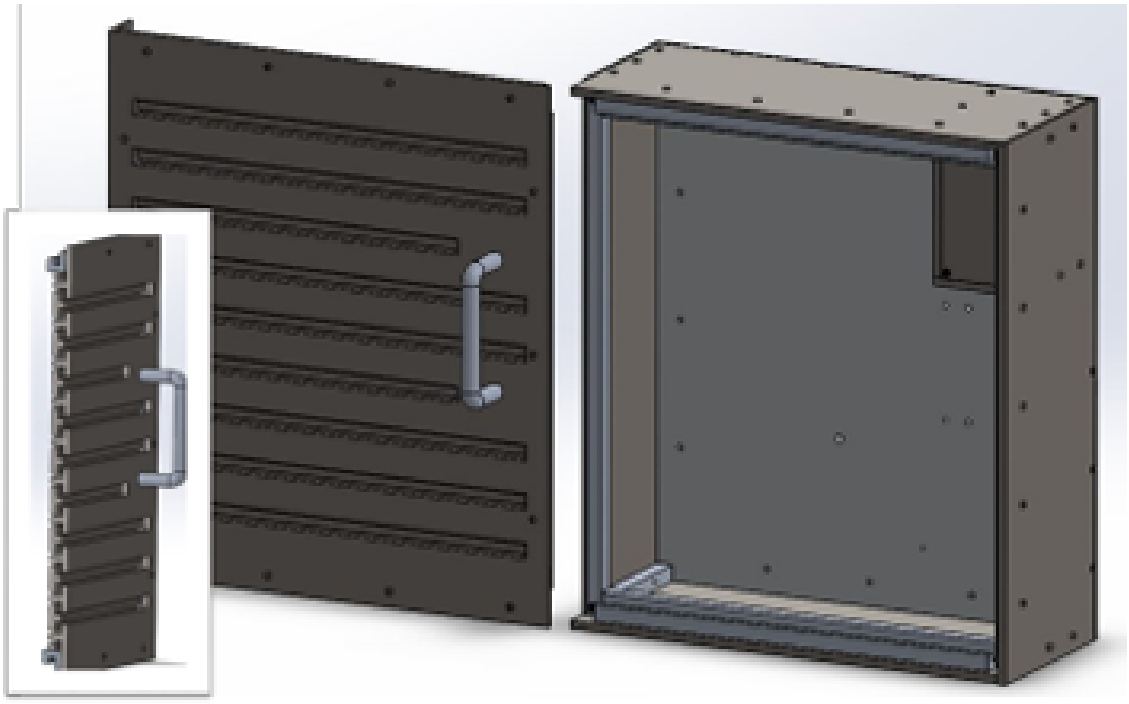

Figure 3.2: Model of the irradiator box developed by the Clemson Medical Physics Lab

Inside of the incubator lies the custom x-ray irradiator cabinet developed by the Clemson Medical Physics lab, as shown in Figures 3.2 and 3.3. This cabinet is made of stainless steel and has measurements of 42.0 cm $\times$ 36.8 cm $\times$ 15.7 cm, allowing it to sit comfortably inside the incubator. The removable front panel is built with radiation blocking slits, allowing for air flow and cooling to occur while still preventing radiation from escaping. In the upper right of the cabinet, a junction box covers all necessary external ports and cable connectors.

3.2 Original Irradiator Set-Up

Now that the build of the irradiator box have been covered, it is important to discuss how the irradiator is set up to actually irradiate targets. I would like to start by discussing the original set-up of the irradiator, and then spend the next section discussing the new changes made to the box.

On top of the box sits an external switch that, when turned on, allows for power to flow to the box. In the center of the box, as shown in Figure 3.4, there is a pivoting mount that holds

Figure 3.3: Irradiator box sitting inside incubator.

a detector and sample mount. The pivoting mount can rotate 20° to either side of the center, and the sample mount can freely rotate. The block holding the sample and detector mounts can be positioned between 30 cm and 170 cm vertically away from the target platform, allowing for both translational and rotational freedom of target placement in the box. The sample holder is an L bracket with an inlaid hole to allow radiation to penetrate through to the target.

The detector is an MXDPP-50 single photon Si-PIN diode detector from Moxtek, Inc. [21]. The detector mount allows it to be placed either in the sample holder or rotated 10° clockwise from the sample. These positions were decided because we wanted the detector to be able to accurately collect calibration data in the position that the target would absorb radiation, and we also wanted the detector to continuously monitor the radiation absorbed during actual experiments while the sample holder was occupied.

At the bottom of the box there is also a mount that holds a target plate. This plate is designed to absorb the bremsstrahlung x-rays produced by the x-ray source and release characteristic x-rays dependent on the type of source plate that is placed onto the mount. The plates that are currently being used are a Ca plate that produces K_α peaks, a Fe plate that releases K_α and K_β peaks, and a Cu plate that releases K_α and K_β peaks. There is also a plate of a powdered multivitamin that can be used that has a known composition and produces peaks of a height proportional to the amount and x-ray-energy-dependent excitation cross section of the given element that is present.

In the top-left corner, pointing directly at the target plate mount, sits our x-ray source. The x-ray source is a commercially-available 4 W x-ray fluorescence tube from Moxtek, Inc.. It produces bremsstrahlung x-rays in a 120° emission cone that are absorbed by the target plate. It is surrounded by shielding to block any extraneous bremsstrahlung x-rays from hitting the detector or target sample. It also has a PCIe slot fan attached near it to help with air flow and cooling.

In order to irradiate cells with the x-ray source, a highly specialized cup was developed. The cells are cultured in high-density polyethylene (HDPE) cups [22] with a 6 μm Mylar® sheet stretched over the bottom. Mylar® was chosen as the bottom material for the cup to limit x-ray attenuation before irradiating the cells. Before use, the both the cup and mylar sheets are sterilized with 100% ethanol, then they are rinsed with a sterile 1X Phosphate Buffered Saline (PBS) solution, and then they are air dried in a standard biological safety cabinet.

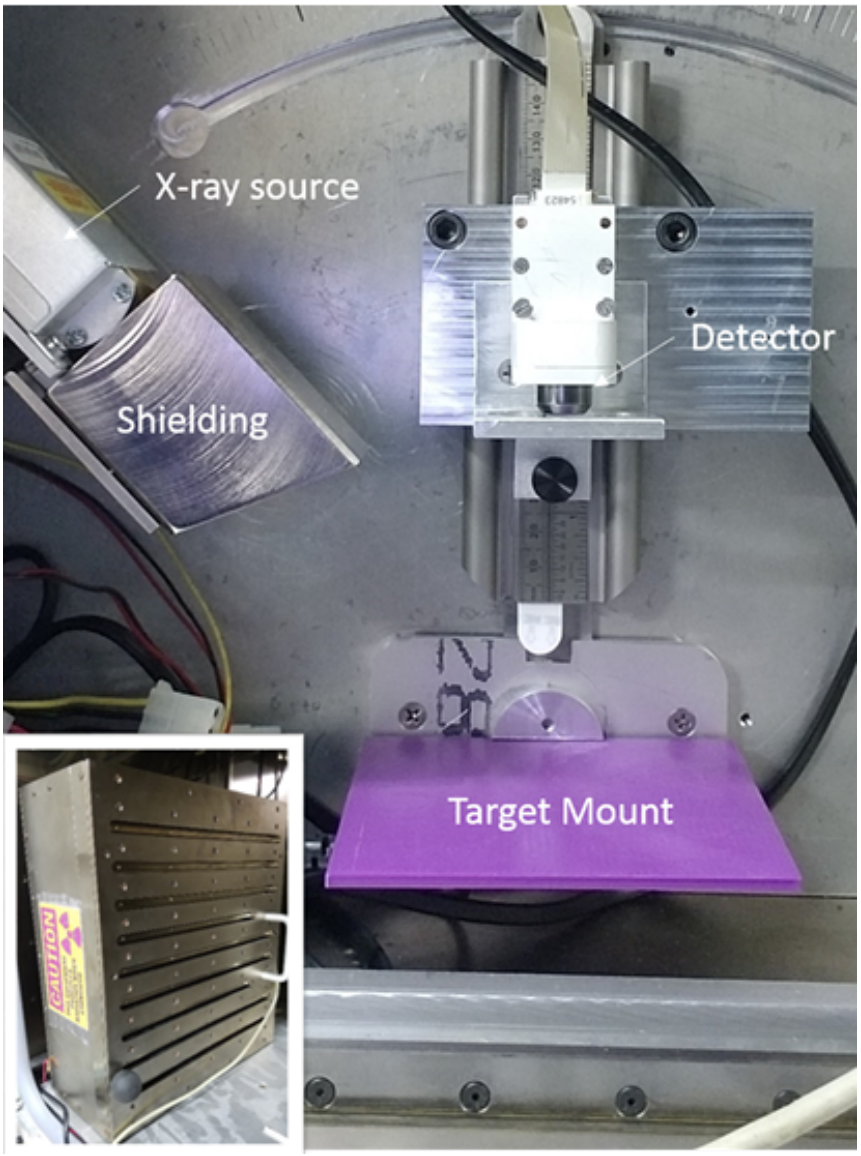

Figure 3.4: Original set-up of the x-ray irradiator cabinet.

3.3 New Irradiator Set-Up

The original set-up is great for delivering highly-characterized, soft x-rays onto cells, however it is limited in the maximum dose that it can impart. This is because the system loses a lot of energy transferring from the bremsstrahlung x-rays to the characteristic x-rays; the efficiency is not great. This limits the types of targets that we can study, as some materials like bone and tissue attenuate low-dose x-rays too easily, not allowing the dose to penetrate all the way through. To remedy this, I redesigned the x-ray system to directly irradiate target cells with bremsstrahlung x-rays. In doing so, a few changes were made to the irradiator box, which can be seen in Figure 3.5.

First, the x-ray source was moved to the site of the old target plate mount. The x-ray source is mounted to the wall using an L-bracket to place it in an upright position, with the source pointing directly at the sample mount. This allows for the source to hit any target directly with the bremsstrahlung x-rays it produces. There is also no shielding surrounding the x-ray tube now, since we don't need to worry about blocking any extraneous bremsstrahlung x-rays. There is also a PCIe fan attached to the back of the L-bracket to help with air flow and cooling.

Second, I had to create a new detector mount. This is for a few reasons. First, the x-ray source in the new position causes the source to be a lot closer to the sample holder/detector. In order to get some added height I wanted to add some extra positions, that way if the detector mount was moved to the max height on the pivoting block I could still increase the height of the sample holder/detector even further. Second, when the detector was in the 10° clockwise position, it was placed to the right of the sample cup. When raising the detector mount, the detector would end up hitting the junction box. So, in order to prevent this, the detector was moved to the left of the sample cup. Unfortunately, there is still a small issue with the detector mount. As seen in Figure 3.5, when the detector is placed directly in line with the sample mount, the detector hits part of the plug that powers itself. For the purposes of this research, this was not an issue, however for future studies it may be important to design a new detector mount that is able to avoid the plug entirely.

Finally, I designed a method to add in filters in between source and the sample mount. This was simply done by screwing two clips into the side of the sample mount. This was done for a couple reasons, first due to the fact that in this position the x-ray source is going to be sending a lot more photons to the detector. Something that I worried about was the detector getting over-saturated, as it was mentioned in previous research that the detector had the potential to get overloaded in the

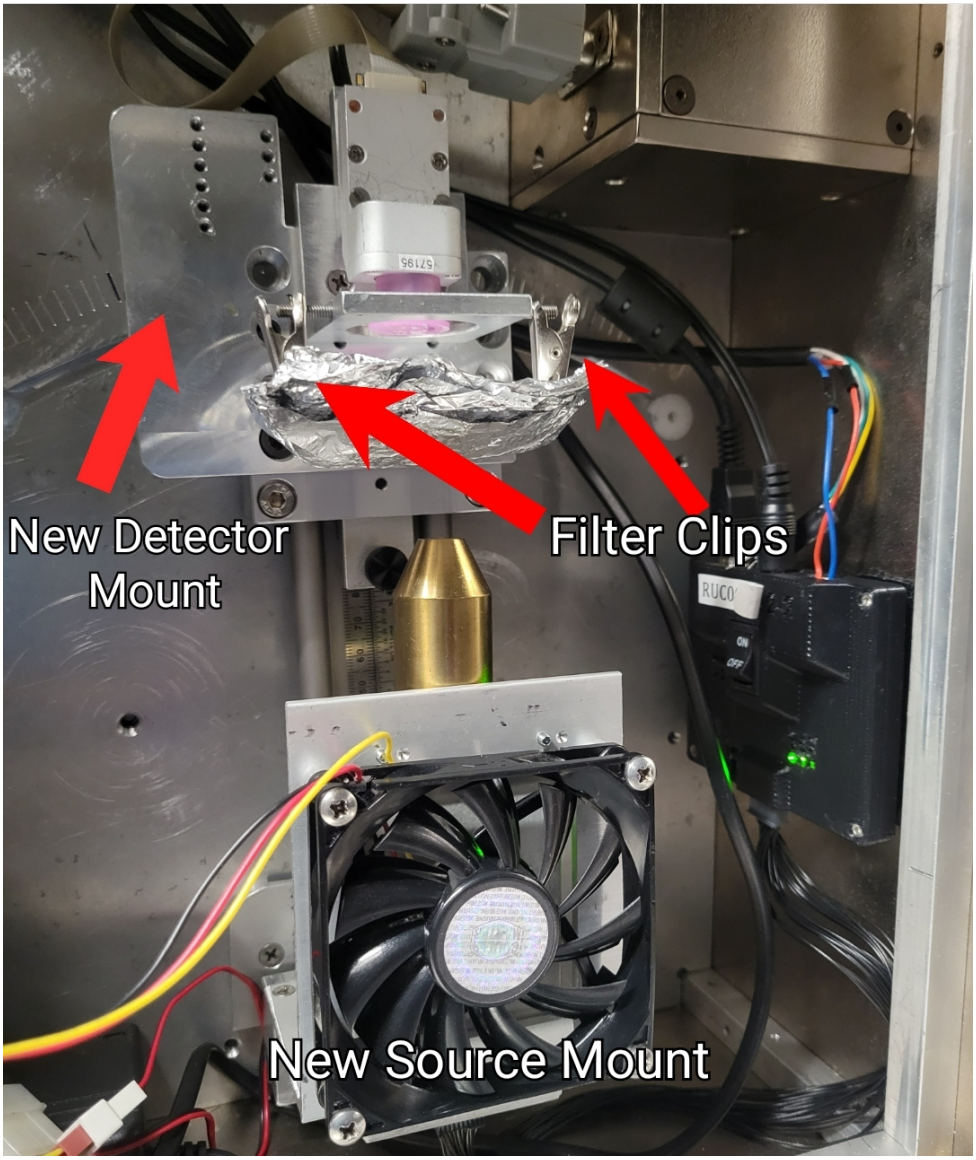

Figure 3.5: New set-up of the x-ray irradiator cabinet.

past [23]. Second, in the previous set-up the only way to limit the dose administered was by either reducing the current or voltage. By mounting a filter, this introduces a new way to alter the dose administered. Since the filter clips are attached to the sample mount directly, this feature can now be used in both the original and the new set-up.

Chapter 4

Understanding the Spectra

Many tests were done in order to understand what physics was occurring in the new set-up. Reported here are the results from multiple irradiations with the detector in the position of the sample holder to collect various spectra.

4.1 Data Collection

I first set up the detector control program, X-Spectrum, and the x-ray source control program, Ringo LifeTime Test. The X-Spectrum program, as shown in Figure 4.1, is a program that takes data from the detector and then plots photon count per detector channel. The program also displays the real time, live time, and dead time of the detector. To use the program, you can set the total time you want to collect under the "DPP" tab of the program. You can also set whether you want the program to time the collection based on the live time or the real time. This is important, since the live time is the counting interval in which radiation interaction in the detector is recorded, while the real time is the time that passes on a clock while the detector runs. The live-time is designed to exclude the dead time from the interval of counting [24].

The Ringo LifeTime Test program, as shown in Figure 4.2, allows the user to set the voltage (in kV) and the current (in μA) of the x-ray source. Setting the voltage allows you to set the max photon energy that is produced, and the current controls how many photons are produced at a time. Once the voltage and current are set, the source is powered on by pressing the X-ray Enable button. As mentioned before, the outside of the incubator has a magnetic interlock that prevents

the irradiator from running if it is unlocked. If this is the case, the text on the X-ray Enable button will lighten, and the button will not be able to be pressed in this state. The x-ray tube temperature is also tracked in the Ringo LifeTime Test program. The tube temperature should avoid going above 40°C to prevent damage to the tube, and also to prevent any damage to cells if they are present during the experiment.

While taking the data there were three parameters that I could alter: The voltage of the x-ray tube, the current of the x-ray tube, and the type/thickness of the filter used. During my runs, I kept two of the variables the same while changing the other, in order to see how each one affects the data individually. For each run, I had it run for 100s live time. Not only did this standardize the run time throughout the experiment, it also allowed me to study the dead time to see how the detector performed throughout the experiments.

4.2 Data Analysis

Pictured in Figure 4.3 is a sample of a spectra collected by the X-Spectrum program. As stated before, the program plots the data by photon count per channel. In order to do any meaningful study on the spectra, it needs to be calibrated. Calibration allows me to determine how much energy is represented by a single channel, which can then be used to see how many photons of each energy were detected. This is important to understand the spectra we are seeing, and it is very important for a dose rate calculation.

Unfortunately, it is currently very difficult to perform a calibration of the detector in the new set-up. However, a calibration done in the old set-up works fine for the detector. A calibration was performed earlier last month by collecting a spectra with the Cu plate in the detector mount, and using the characteristic peaks to determine what energies align with each channel. Using this calibration, the energies of each photon detected was found.

With the calibration completed, the data collected could now be accurately studied. First, I irradiated using four different filters. Pictured in Figure 4.4, the filters used were Al, Pb, Fe, and Cu. The voltage, current, and thicknesses of each filter used during the initial tests are listed in the Table 4.1:

The Al filter was tested at a different voltage and current than the other three tests because at the higher levels of voltage (15 kV) and current (200 μA), the detector got immediately overloaded

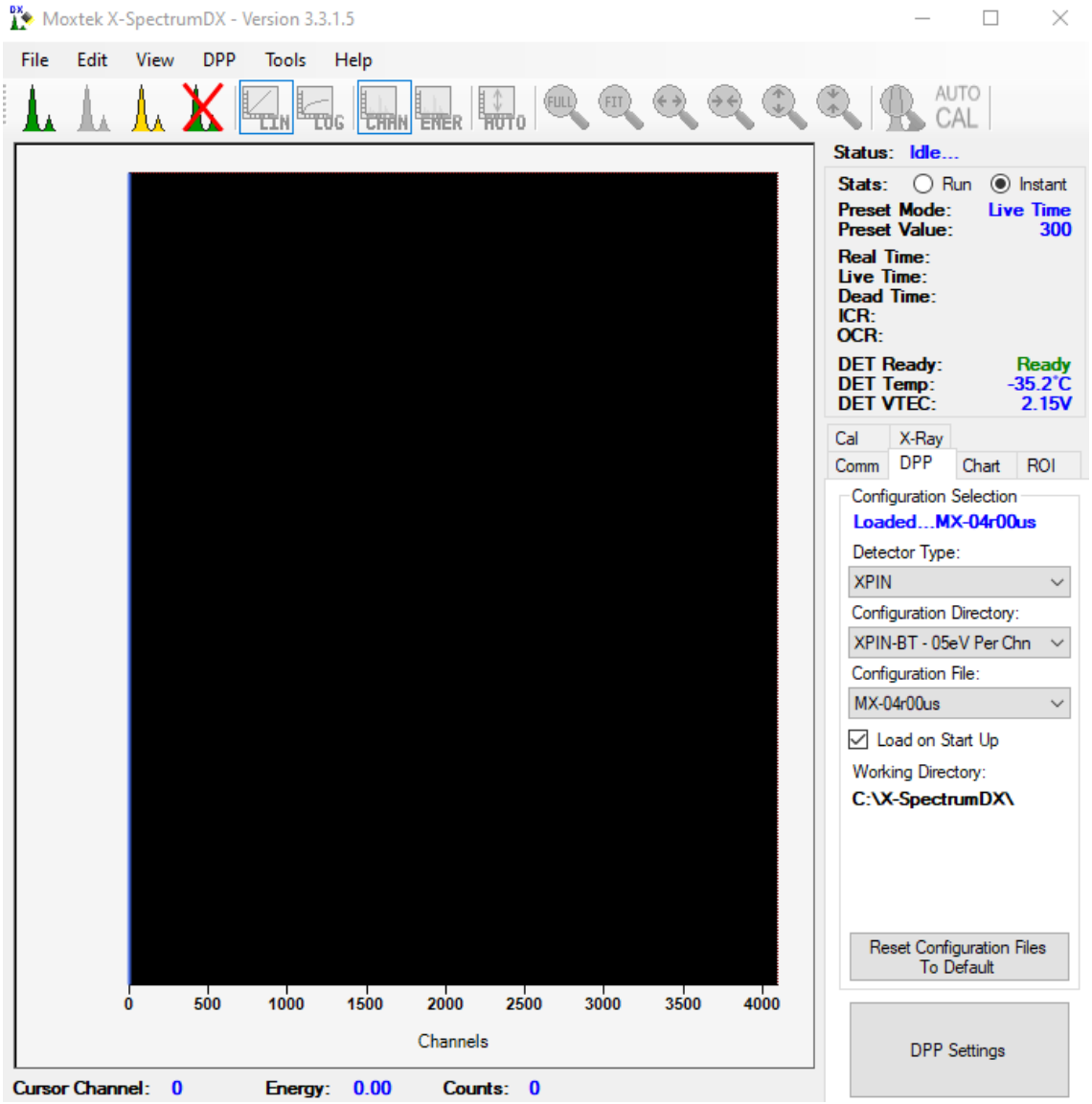

Figure 4.1: The detector control program, X-Spectrum. To start data collection, you click the green spectra button in the top left corner. In the top right corner, it records the real time, live time, and dead time of the detector.

Filter	Voltage (kV)	Current (μA)	Thickness (mm)
Al	10	10	0.08
Pb	15	200	0.71
Fe	15	200	0.55
Cu	15	200	0.80

Table 4.1: Experimental parameters for the four different filter tests.

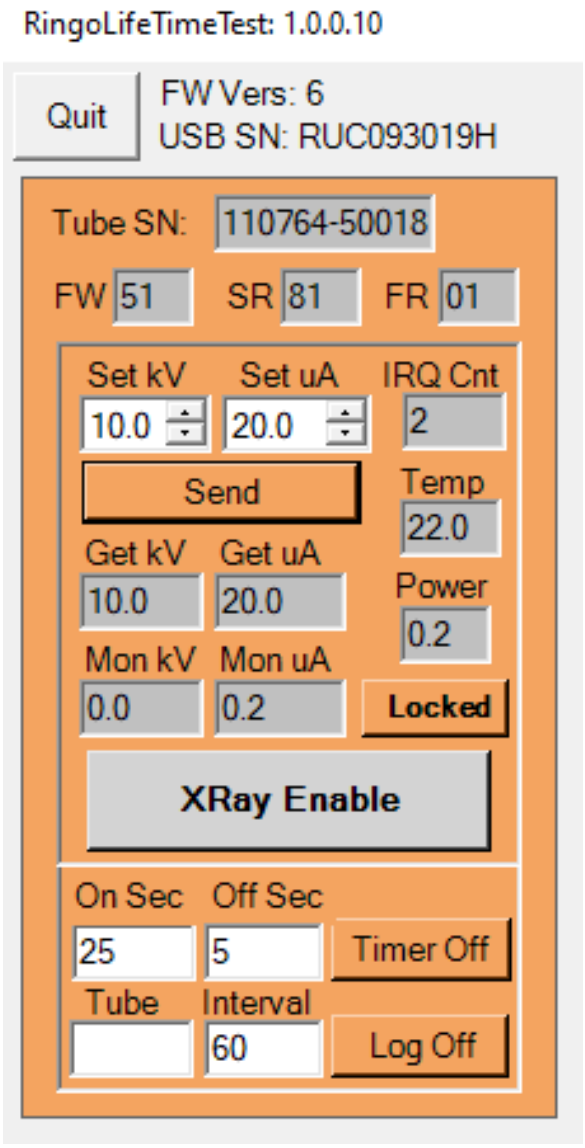

Figure 4.2: The x-ray source control program, Ringo Lifetime Test. In this program you set the desired voltage and current using the "set kV" and "set uA" buttons, respectfully. To tell the source to start producing x-rays, you press the gray "X-ray Enable" button. You can also see the tube temperature on the right-hand side in the "Temp" box

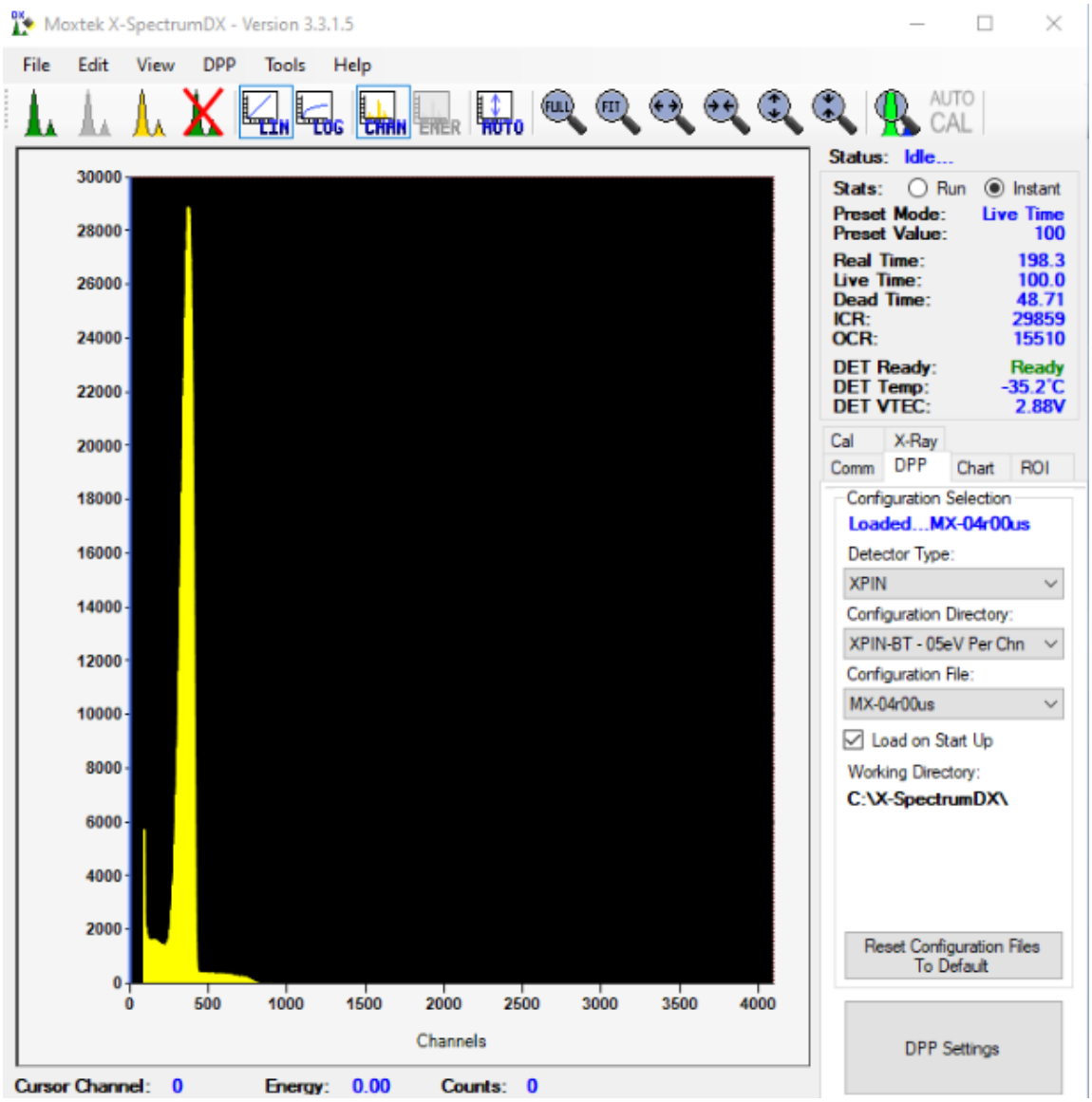

Figure 4.3: A sample spectra collected using the X-Spectrum program. It is a graph of Counts vs. Detector Channel.

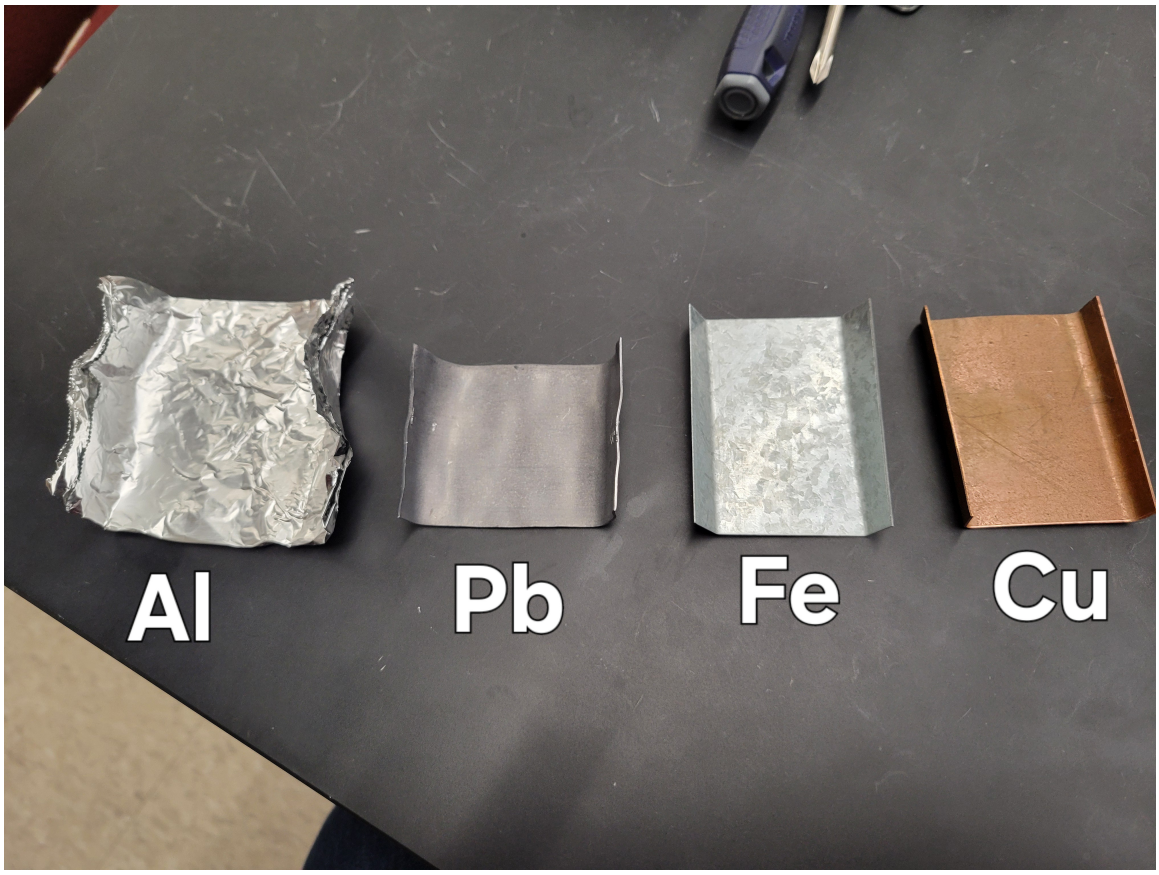

Figure 4.4: The four different filters used in testing the irradiator.

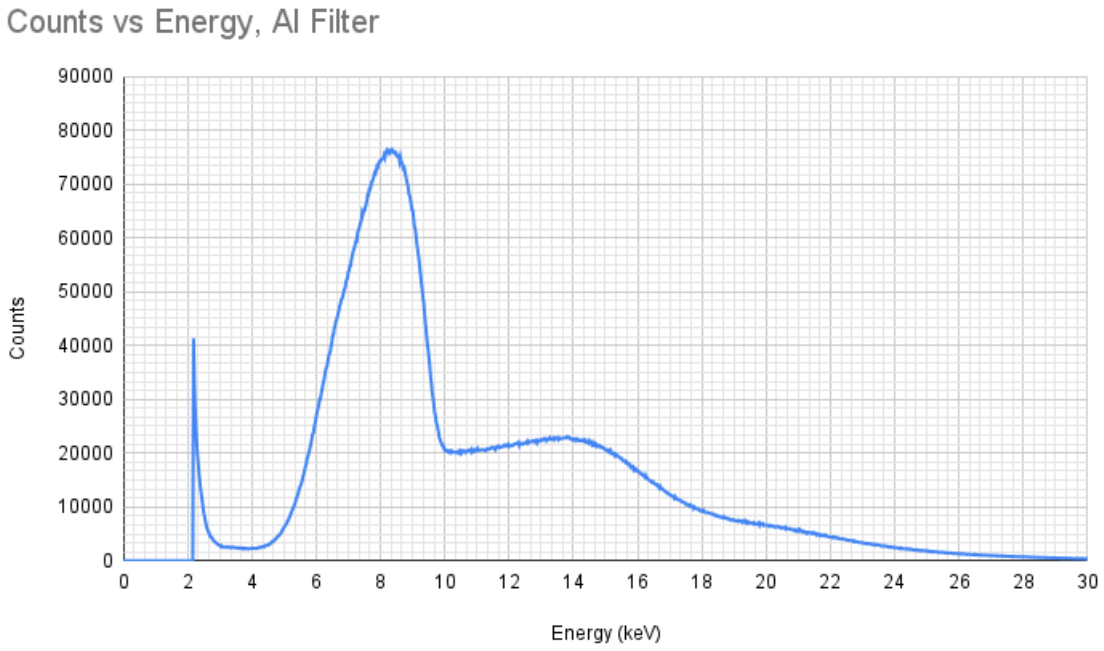

Figure 4.5: 0.08 mm Al filter spectra.

and stopped working properly. The resulting spectra are shown in Figures 4.5, 4.6, 4.7, 4.8

Immediately, it is seen that the counts for the aluminum are much higher. This makes sense, as the thickness of the aluminum is a lot thinner. Second, in all four of the graphs, it is seen that there are some dips in the spectra. Bremsstrahlung x-rays are supposed to be a smooth, continuous spectra, so the fact that there are dips in the spectra means that those specific energies are being blocked somehow. One possible explanation for this is that, as discussed in Chapter 2, x-rays get attenuated when passing through a medium. The way that the x-rays get attenuated is material dependent, so in order to confirm this theory I checked the transmission coefficients of each of the filters, as seen in Figure 4.9. When looking at the transmission curves of each of the elements, it can be seen that there are certain cutoff points where the transmission dips. Comparing the spectra to the transmission, it is clear that there is some connection. For example, in the Fe filter, there is a dip around 7 keV in the spectra, and on the transmission graph there is a slight cutoff, and in all 4 transmission graphs it shows there is a lot more attenuation for lower energies, which is consistent with the spectra seen. However, this does not explain every dip in the collected spectra, as the transmission graphs are not 100% consistent. One possibility for this is that the filters are not pure

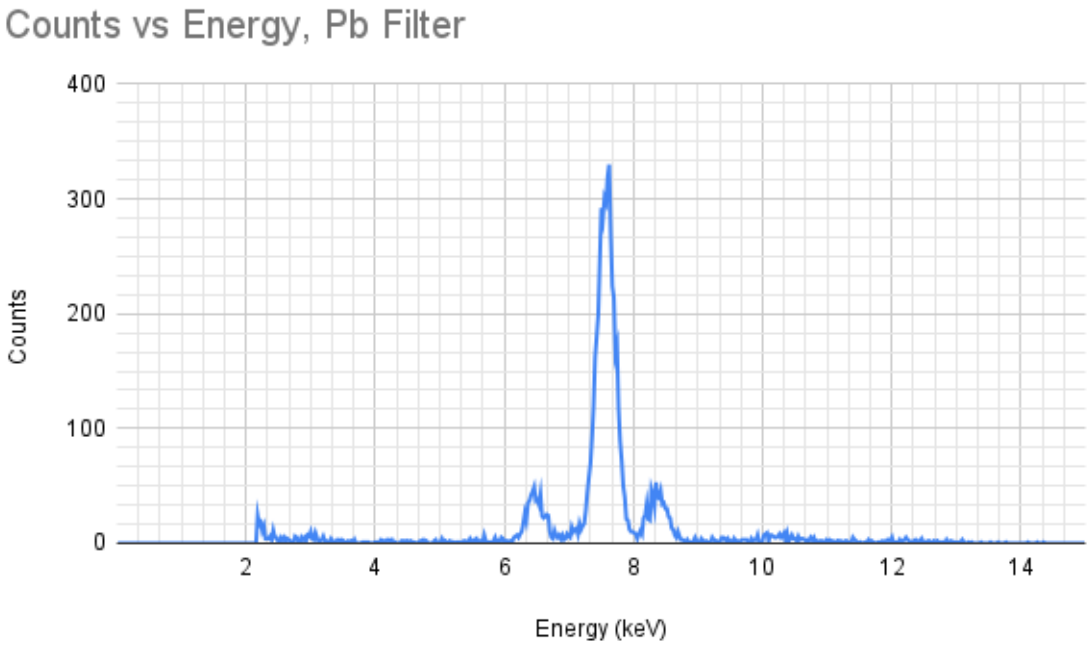

Figure 4.6: Pb filter spectra.

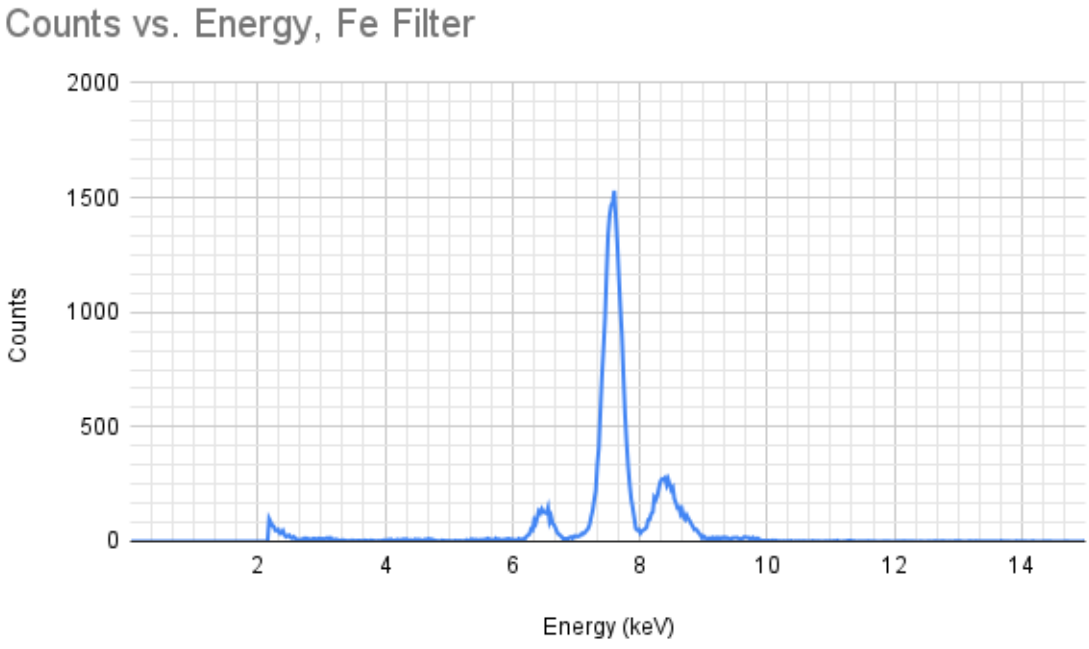

Figure 4.7: Fe filter spectra.

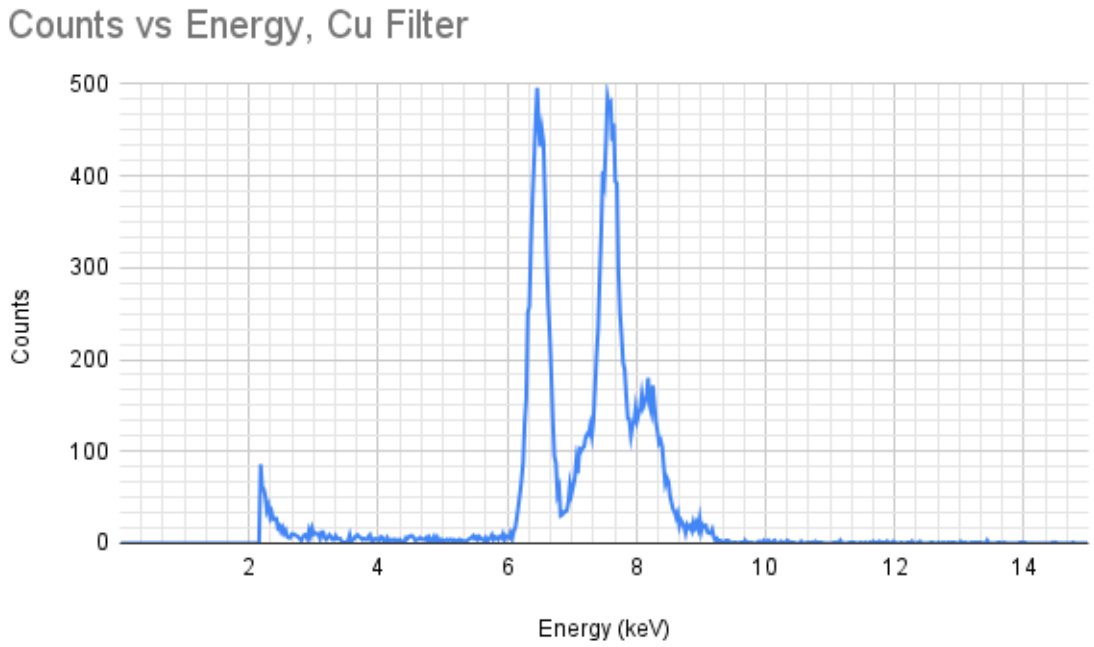

Figure 4.8: Cu filter spectra.

elements, rather they are alloys. Because of this, there are dips in places that may not show up in the transmission graphs, since the graphs are based on only singular elements.

Another interesting feature is seen in the Al filter spectra in Figure 4.5. Looking at the graph, it seems that the photon energies seem to extend well into the 20 keV range and beyond. However, the voltage was initially set to 10 kV, which means the maximum energy that a photon from the source should have is 10 keV. It was initially concerning that there were these "impossible" photons appearing in the spectra. A couple possibilities arose to explain this discrepancy. One is that the calibration done on the spectra was incorrect. The other, arguably more likely case, is that the photons we were seeing was actually the detector accidentally double or triple counting photons. There is a possibility that, if a detector is being bombarded by too many photons, it can actually detect two or three photons at the same time. In order to figure out what was causing this feature, more spectra need to be studied.

Another test done while studying the irradiator was altering the thickness of the Al filter. Because the Al filter is so thin (one sheet = 0.02 mm), it is possible to stack many sheets on top of each other, allowing for variable thickness. To test the effects of the thickness on the spectra, I

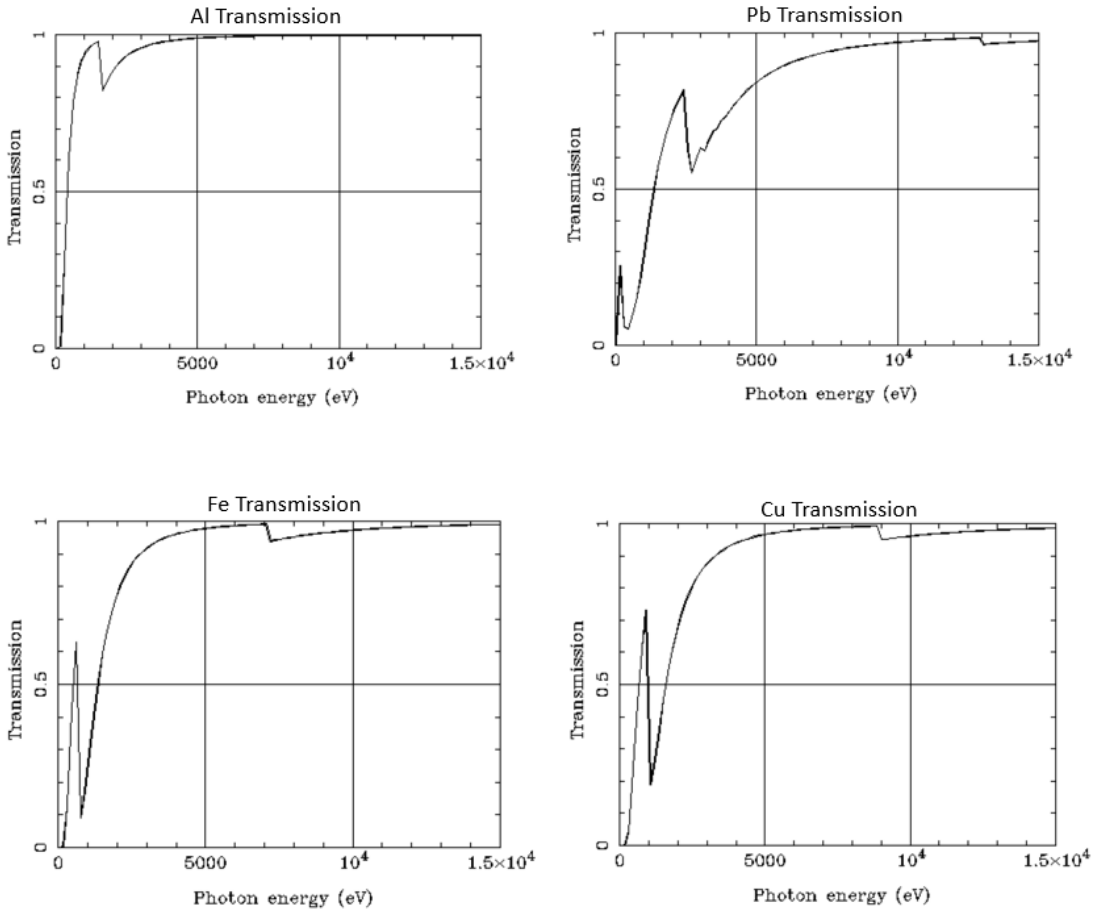

Figure 4.9: Transmission coefficients of each of the filters [25].

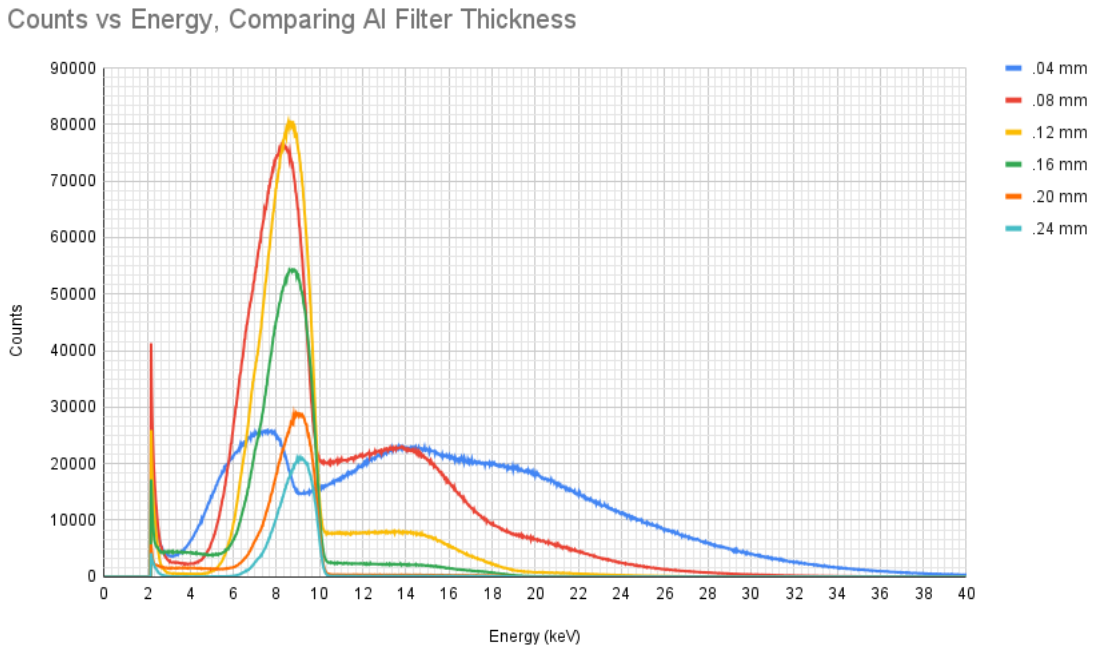

Figure 4.10: Spectra taken with various Al filter thicknesses, at 10 kV and 10 μA

started with an Al thickness of 0.04 mm, and increased in steps of 0.04 mm until I reached a filter thickness of 0.24 mm, while keeping the voltage at 10 kV and the current at 10 μA. The results of this test can be seen in Figure 4.10

There are a couple features of the spectra worth noting. First, when looking at the relationship between the thickness of the Al filter and the "impossible" photons, it is clear that as the thickness of the filter increases, the amount of these photons decreases until they are completely eliminated at a thickness of 0.20mm. This is a good indication that the feature we are seeing in the spectra is just an artifact of the detector timimg resolution. Second, looking at the first peak in each of the spectra, if you look at where each of them ends, it is right around 10 keV. This is a sign that the calibration is correct, since that is the expected energy that the highest energy photons should have due to the 10 kV voltage setting.

Another test that was done was changing the voltage of the x-ray tube while keeping the current and the thickness of the Al filter the same. The voltage was started at 5 kV, and went up in 1 kV increments until a final voltage of 10 kV. The current was kept at 10 μA, and the thickness of the Al filter was 0.04 mm. The results of this test can be seen in Figure 4.11

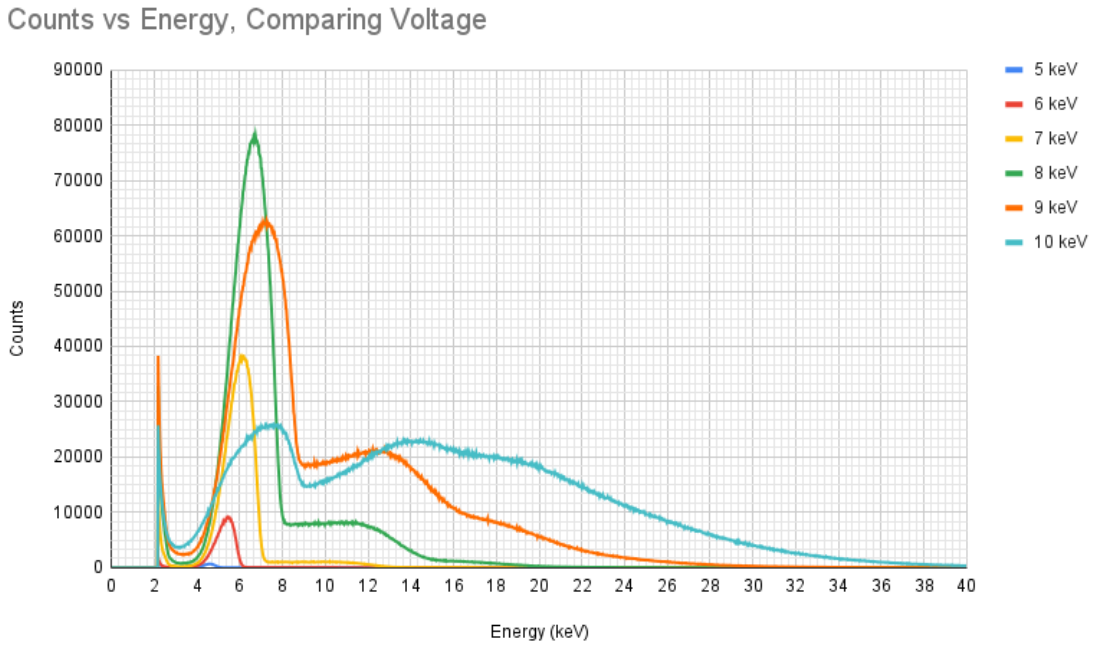

Figure 4.11: Spectra taken at various voltages, at 10 μA and an Al filter thickness of 0.04 mm

Looking at the spectra produced with the different voltages, it is consistent with what was discussed in our previous results. We can see that the main peak of each of the spectra cuts off at the respective max energy that is expected from of the voltage setting. Furthermore, it is seen through the spectra that there is a voltage dependency on the amount of double and triple photon counts we see; as the voltage increases, the double and triple photon counts increase as well.

The final test that was done was changing the current of the x-ray tube while keeping the voltage and the thickness of the Al filter the same. The current was tested at 4 μA, 10 μA, 15 μA and 20 μA. The voltage was kept at 10 kV, and the thickness of the Al filter was 0.08 mm. The results of this test can be seen in Figure 4.12.

The results of this test seem to further support the previous claim, since the main peak ends at the expected 10 keV energy. It seems like there is a slight dependence between the current and the amount of double/triple counting photons. Something else that is interesting to note, is that although the current increases, the total counts under the main peak does not proportionally increase. It looks like the total counts under the main peak caps at around 10 μA, and then decreases for 15 μA and 20 μA. I believe this is due to the fact that as the current increases, more photons are

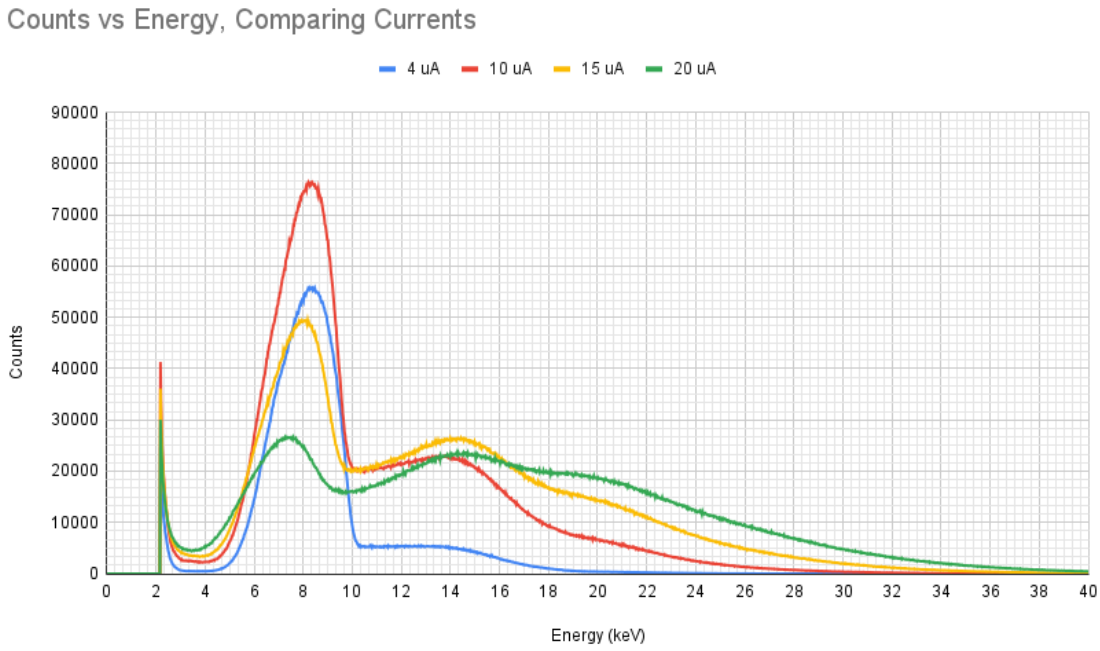

Figure 4.12: Spectra taken at various currents, at 10 kV and an Al filter thickness of 0.08 mm

being detected as a double and triple count photon. This makes sense, since as the current increases there should be a higher production of photons, meaning it is more likely that the detector can get overloaded.

Overall, the first results from the new x-ray irradiator set-up look very promising. Everything seems to be working properly, and it is producing expected results, as seen in the spectra provided. There is the issue of double and triple counting photons of the detector that can have an effect on future calculations if not fully understood properly, however it is clear that these artifacts can be avoided if the right steps are taken. By using a thicker filter, lower voltage, or lower current, it can reduce or fully diminish the amount of double and triple counted photons seen, allowing for a clean spectrum. This is a great leap in progress for the irradiator, however there is still more work to be done.

Chapter 5

Future Work

Although much work has been done on the x-ray irradiator, there is plenty more that can be done in the future to further help research on low-dose x-ray irradiation. Ultimately, the goal is to start irradiating cells in the new set-up, however there are still a couple of steps that need to be done before it is ready to do so.

The first, and arguably most important, thing to be done is to develop a program to easily calculate the dose rate being administered from the spectra provided. You can theoretically derive the dose rate from Equation 2.12 by dividing the absorbed dose by the total time taken to irradiate using the following equation:

$$\frac{D}{\Delta t} = \sum_i \frac{N_i E_i}{M * \Delta t} \tag{5.1}$$

However, this does not take into account any corrections that need to be made to the photon count. There are many corrections that need to be made to the photon count, including the transmission coefficients of the air, Be window, and filter that the photons pass through to get to the detector, the correction between dead time and real time, the transmission coefficients of the air and the Mylar® that the x-rays pass through to get to the cells, and the absorption coefficient of the cells (which can be generally approximated to have the same coefficient as water). This leads to a final equation of

$$\frac{D}{\Delta t} = \sum_i \frac{N_i E_i C_i}{M * \Delta t} \tag{5.2}$$

where C_i is the correction factor to the photon counts:

$$C_i = T_{iAir1} * T_{iMylar} * T_{iFilter} * (1 - T_{iWater}) * [1 + (1 - T_{iBe})] * [1 + (1 - T_{iAir2})] * C_d \qquad (5.3)$$

where T_i represents the transmission coefficients for each material, calculated using Equation 2.16, and C_d is the correction for dead time, which is just the dead time divided by the real time (t_d/t_r). For the old set-up, there is currently an excel sheet set up to calculate the dose rate, however it needs to be heavily modified in order to be used for the bremsstrahlung x-ray spectra being produced in the new set-up. There is also the possibility of doing a complete overhaul of the excel sheet to develop a new code that can analyze both characteristic x-ray spectra and bremsstrahlung x-ray spectra with ease. One major downfall with using the excel sheet is that in order to use the excel sheet an extra calculation has to be done in another program to find the heights and width of each characteristic peak. If a code can be developed, there is the possibility to streamline the process so that the only input needed by the user is to provide the spectra in order to get the dose rate calculation.

Another area of improvement for the irradiator is, using the original set-up, placing the newly produced filters on the target plate mount to get a characteristic x-ray spectrum from them. Using this characteristic x-ray spectrum, one could identify the true composition of the filters. From the results of my research, I believe ever filter used is some type of alloy. In order to make the most accurate dose calculation, it is of utmost importance to know exactly what elements are in each filter so the correction factor can be applied.

As stated in Chapter 3, there was also the issue of the detector hitting its own plug when placed in the sample mount position. In order to fully utilize the space of the box, it is important that a fix is found for this. I believe there may be potential for the fix by rotating the detector in some way to avoid the plug, however not much research has been done on this potential fix yet. Once all three of these issues has been solved, I believe that the x-ray irradiator should be all ready to start irradiating cells.

Chapter 6

Conclusion

Understanding the effects of low-dose radiation is truly important, since the effects of this radiation is still not fully understood. Gaining a better understanding of how x-ray irradiation works can help people avoid unnecessary harm, or even help discover new ways to help the body heal and recover. Experiments done previously in the Clemson Medical Physics lab have helped expand knowledge on low-dose x-ray irradiation, and it is important to continue to drive that research through innovation.

The x-ray irradiator developed previously by the Clemson Medical Physics lab did a great job at delivering very low doses to samples, but struggled to deliver anything higher than a few mGy. In order to improve upon this, a new, interchangeable, set-up was devised for the irradiator. The main difference between the two is that the original set-up delivers x-ray irradiation through characteristic x-rays from target plates, while the new set-up allows the target to be hit with bremsstrahlung x-rays produced directly from the x-ray source.

In this new set-up, one can control the flow of x-rays from the source to the target by altering the voltage, current, or type and thickness of filter used. Studies of spectra taken in this new set-up show that there is a higher chance of the detector accidentally double or triple counting photons which could affect overall dose rate calculations, however this can be avoided by lowering the voltage or current, or by using a thicker filter. There is also evidence that the filters used are comprised of alloys, not pure metal, and in order to get an an accurate dose calculation the composition of the filters needs to be further studied. Besides these two issues, the set-up appears to be in working order.

There are a couple more steps that need to be taken in order to be able to irradiate cells in the new set-up. The first is developing a new program to accurately calculate the dose rate. The second is fully characterizing the filters so their composition can be learned. Finally, although not a necessary requirement, a new detector mount needs to be developed in order to fully utilize the box. Once these changes have been made, the irradiator should be ready to go perform experiments on cells. The Clemson Medical Physics lab has consistently been at the forefront of low-dose x-ray radiation studies, and with this new development the group should be able to continue to do great research.

Bibliography

[1] Weizhong Dai, Haojie Wang, Pedro M Jordan, Ronald E Mickens, and Adrian Bejan. A mathematical model for skin burn injury induced by radiation heating. *International Journal of Heat and Mass Transfer*, 51(23):5497–5510, 2008.

[2] Elizabeth H Donnelly, Jeffrey B Nemhauser, James M Smith, Ziad N Kazzi, Eduardo B Farfan, Arthur S Chang, and Syed F Naeem. Acute radiation syndrome: assessment and management. *Southern Medical Journal*, 103(6):541, 2010.

[3] Arifumi Hasegawa, Koichi Tanigawa, Akira Ohtsuru, Hirooki Yabe, Masaharu Maeda, Jun Shigemura, Tetsuya Ohira, Takako Tominaga, Makoto Akashi, Nobuyuki Hirohashi, Tetsuo Ishikawa, Kenji Kamiya, Kenji Shibuya, Shunichi Yamashita, and Rethy K Chhem. Health effects of radiation and other health problems in the aftermath of nuclear accidents, with an emphasis on fukushima. *The Lancet*, 386(9992):479–488, 2015.

[4] Fred A Mettler. Medical effects and risks of exposure to ionising radiation. *Journal of Radiological Protection*, 32(1):N9, mar 2012.

[5] L E Feinendegen. Evidence for beneficial low level radiation effects and radiation hormesis. *The British Journal of Radiology*, 78(925):3–7, 2005.

[6] Katalin Lumniczky, Nathalie Impens, Gemma Armengol, Serge Candéias, Alexandros G. Georgakilas, Sabine Hornhardt, Olga A. Martin, Franz Rödel, and Dörthe Schaue. Low dose ionizing radiation effects on the immune system. *Environment International*, 149:106212, 2021.

[7] Heather Douglas. Science, hormesis and regulation. *Human & Experimental Toxicology*, 27:603–7, 08 2008.

[8] Shaweta Mohan and Vibha Chopra. Chapter 18 - biological effects of radiation. In Sanjay Dhoble, Vibha Chopra, Vinit Nayar, George Kitis, Dirk Poelman, and Hendrik Swart, editors, *Radiation Dosimetry Phosphors*, Woodhead Publishing Series in Electronic and Optical Materials, pages 485–508. Woodhead Publishing, 2022.

[9] Katelyn Truong, Suzanne Bradley, Bryana Baginski, Joseph R. Wilson, Donald Medlin, Leon Zheng, R. Kevin Wilson, Matthew Rusin, Endre Takacs, and Delphine Dean. The effect of well-characterized, very low-dose x-ray radiation on fibroblasts. *PLoS ONE*, 13(1), 2018.

[10] Nikhilesh S. Bajaj and Chetan B. Palan. Chapter 5 - understanding osl radiation dosimetry and its application. In Sanjay Dhoble, Vibha Chopra, Vinit Nayar, George Kitis, Dirk Poelman, and Hendrik Swart, editors, *Radiation Dosimetry Phosphors*, Woodhead Publishing Series in Electronic and Optical Materials, pages 99–128. Woodhead Publishing, 2022.

[11] D. L. Bailey. *Nuclear Medicine Physics : A Handbook for Teachers and Students*. IAEA, 2015.

[12] Office of Environment, Health, Safety, and Security. The doe ionizing radiation dose ranges chart, Feb 2018.

[13] James S. Walker. *Physics*. Pearson, 2017.

[14] John David Jackson. *Classical Electrodynamics*. Wiley, 1998.

[15] Martin Berger, Qiao Yang, and Andreas Maier. Chapter 7: X-ray imaging. In A. Maier, S. Steidl, V. Christlein, and et al., editors, *Medical Imaging Systems: An Introductory Guide [Internet]*. Cham (CH): Springer, 2018.

[16] Motohiro Uo, Takahiro Wada, and Tomoko Sugiyama. Applications of x-ray fluorescence analysis (xrf) to dental and medical specimens. *Japanese Dental Science Review*, 01 2014.

[17] PhysicsOpenLab. Bremsstrahlung radiation, Aug 2017.

[18] Muhammad Maqbool. *An introduction to medical physics*, volume 1. Springer International Publishing, 2017.

[19] D. R. Dance, S. Christofides, A. D.A. Maidment, I. D. McLean, and K. H. Ng. *Diagnostic Radiology Physics: A handbook for teachers and students*. IAEA, 2014.

[20] Fisher Scientific. Isotemp microbiological incubator.

[21] Moxtek Inc. Xpin-13xt x-ray detector.

[22] Chemplex Industries Inc. HDPE Cup.

[23] Jaclyn D'Avanzo. Delivering highly-characterized low-dose x-ray radiation to biological samples, August 2021.

[24] Ching Y. Chen and Robery Y.L. Chu. Can a detector in live-time mode give a true count rate? *JOURNAL OF NUCLEAR MEDICINE TECHNOLOGY*, 18(1):38–39, 1990.

[25] Eric Gullikson. X-ray interactions with matter, 1995-2024.